# Combined Two-phase Co-flow and Counter-flow in a Gas Channel/Porous Transport Layer Assembly

S. B. Beale<sup>a,b</sup>, M. Andersson<sup>c</sup>, N. Weber<sup>d</sup>, H. Marschall<sup>e</sup>, and W. Lehnert<sup>a,f</sup>

 <sup>a</sup> Forschungszentrum Jülich GmbH, 52425 Jülich, Germany
 <sup>b</sup> Department of Mechanical and Materials Engineering, Queen's University, Kingston ON K7L, 3N6, Canada

Department of Energy Sciences, Lund University, 22100 Lund, Sweden
 Institut für Fluiddynamik, Helmholtz-Zentrum Dresden-Rossendorf e.V., 01328
 Dresden

e Thermo-Fluids and Interfaces, Technische Universität Darmstadt, Alarich-Weiss Straße 10, 64287 Darmstadt, Germany f RWTH Aachen University, 52056 Aachen, Germany

This paper considers a detailed numerical analysis of combined liquid-gas co-flow in a gas channel, with liquid-gas counter-flow in a porous transport layer, as is typically found on the cathode side of a polymer electrolyte fuel cell. The geometry is obtained by digital reconstruction of nano-computer tomography images. From this, the domain is tessellated with an unstructured castellated or octree mesh, upon which the equations of mass and momentum are solved by means of a volume of fluid method. Liquid water is produced from an electrode where gaseous oxygen is simultaneously consumed by electrochemical reduction; Liquid-gas counter flow in the porous transport layer results in liquid drops being entrained in co-flow in the gas channels and convected by the gas downstream.

#### Introduction

Both water electrolyzers and fuel cells, based on polymer electrolyte membrane technology are the subject of much attention, at present. Numerical analysis of electrochemical processes and devices has, together with analytical and experimental work, formed a cornerstone for applied research and development. Until recently, detailed analysis of twophase flow phenomena has proved difficult or impossible to realize, due to limitations in computational resources. Calculations for multi-phase flow phenomena may be performed, for example using popular Eulerian-Eulerian (1, 2) and Eulerian-Lagrangian (3) approaches, typically based on additional closure assumptions. Wang and Cheng (4, 5) considered a so-called mixture model to describe the motion of a mixture of two phases in the porous layers of a polymer electrolyte fuel cell (PEFC), whereas Gurau et al. (6) solved the PEFC problem with an Eulerian-Eulerian methodology similar to that developed previously by Lo and Spalding (7). Although, theoretically, such approaches can distinguish between two or more phases, in practice the phase boundaries become smeared due to volume-averaging and numerical diffusion, and each computational cell has volume fraction for phase i,  $\alpha_i$ , such that  $0 \le \alpha_i \le 1$  without any precise knowledge of the distribution of i within the cell. Conversely, in volume of fluid (VOF) methods, the interphase surface distinguishes the two (or more) immiscible phases. Le and Zhou (8) employed a commercial code to perform two-phase calculations in the serpentine passages of a PEFC. Andersson et al. (9-12) modeled drop dynamics in PEFC gas channels under various conditions of static and dynamic contact angles with experimental validation. Niblett et al. (13) considered water drainage through the both ordered and random porous transport layers (PTLs) and subsequent entrainment by the gas in the channel of a PEFC.

### **Problem Statement**

### Geometry and mesh construction

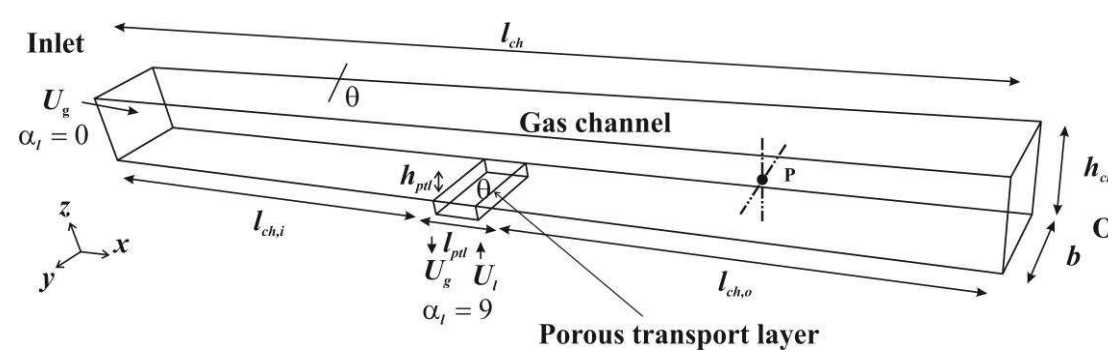


Figure 1. Schematic of problem under consideration (not to scale).

The geometry considered is in the form of a 'T-shape' with the porous transport layer (PTL) in the form of a thin rectangular prism of dimensions  $0.5 \times 0.5 \times 0.1$  mm<sup>3</sup> located at the base of the 'T', and the gas flowing across the top in the channel, in the *x*-direction, as shown in Fig. 1. TABLE I provides details of the geometry considered. The PTL is reproduced by digital reconstruction of nano-computer tomography images of a Freudenberg H2315 PTL in the form of a stereolithography file, see Fig. 2 (a). From this, the domain is tessellated with an unstructured castellated, or octree, type mesh, Fig. 2 (b). The open source software snappyHexMesh was employed to construct a mesh of  $7.8 \times 10^6$  computational cells, for the work described in this paper.

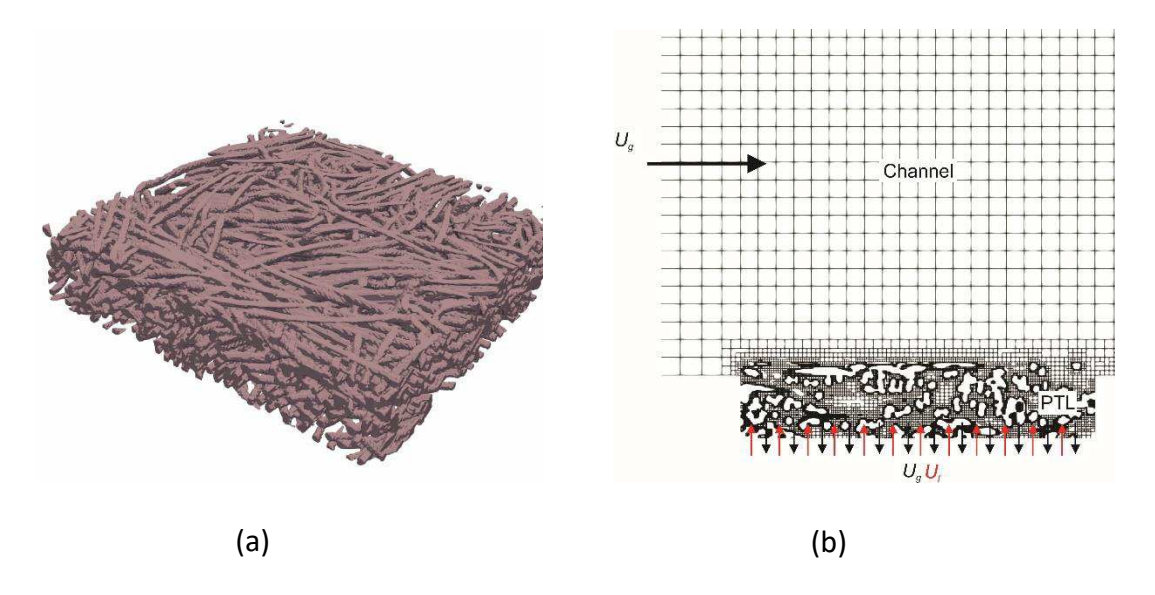


Figure 2. (a) Detail of a digitally reconstructed Freudenberg H2315 porous transport layer. (b) Two-dimensional slice of the castellated mesh, showing both channel and porous transport layer regions in a centre-plane corresponding to the main flow direction.

## Volume of fluid method

The VOF method is applied to the problem-at-hand. It is assumed that the liquid phase is water, H<sub>2</sub>O, and that the gas phase is pure oxygen, O<sub>2</sub>, and that this system constitutes two immiscible fluid phases of high density and viscosity contrast, i.e. a gas-liquid system. In future, the underlying assumptions might be relaxed so as to allow for injection/removal of pure oxygen to/from atmospheric air by means of the continuous surface transfer model (14). Herein, the two-phase fluid dynamics are extended consistently by a model for interfacial species transfer within the VOF methodology. Figure 1 is a schematic of the present problem. For the case depicted, it is assumed that gaseous oxygen is consumed and liquid water produced at the cathode surface (oxygen electrode), in the z-direction. Gravity acts in the -z direction.

The algebraic VOF approach used here, belongs to the family of interface capturing methods. The interfacial flow is governed by the two-phase Navier-Stokes equations in single-field formulation. This can be derived by means of a conditional volume-averaging technique from the local Navier-Stokes equations (15), taking into account jump and transmission conditions for mass and momentum at the fluid interface. The closed form reads, for incompressible flow:

$$\operatorname{div}(\boldsymbol{U}) = 0 \tag{1}$$

$$\operatorname{div}(\boldsymbol{U}) = 0 \tag{1}$$

$$\frac{\partial \alpha}{\partial t} + \operatorname{div}(\alpha \boldsymbol{U}) = 0 \tag{2}$$

and

$$\frac{\partial(\rho U)}{\partial t} + \operatorname{div}(\rho U U) = -\operatorname{grad} \overline{p} + \overline{\rho} g + \operatorname{div}(\overline{\mu}\operatorname{grad} U) - \sigma \operatorname{div}\left(\frac{\operatorname{grad} \alpha}{|\operatorname{grad} \alpha|}\right) \operatorname{grad} \alpha \qquad (3)$$

where  $U = \alpha_l U_l + \alpha_g U_g$ . For closure, the homogeneous mixture model has been employed, i.e. no interphase slip of the phasic velocities,  $U_g - U_l = 0$ . Thus, the barycentric mixture velocity  $\tilde{U} = (\alpha \rho_l U_l + \alpha \rho_g U_g)/\rho$  becomes equivalent to the volumetric mixture velocity  $U_s$ . The mixture density and dynamic viscosity are defined as volume-averages:

$$\rho = \alpha_1 \rho_1 + \alpha_{\sigma} \rho_{\sigma} \tag{4}$$

$$\mu = \alpha_I \mu_I + \alpha_\sigma \mu_\sigma \tag{5}$$

To include capillarity of the fluid interface, the continuous surface force model of Brackbill et al. (16) is employed to close for the volumetric surface tension force, i.e.,  $M_{\sigma} = -\sigma \operatorname{div} \left(\operatorname{grad} \alpha/|\operatorname{grad} \alpha|\right) \operatorname{grad} \alpha$ . A number of advection schemes have been described in the literature for the volumetric phase fraction transport equation, Eq. (2). In this study the multidimensional universal limiter with explicit solution scheme was employed. This enforces boundedness and sharpness of the volumetric phase fraction field by means of flux corrected transport, iteratively (17-19). Alternatives are to use specialized high resolution schemes, so-called interface capturing schemes, such as the interface capturing scheme on arbitrary meshes by Ubbink and Issa (20) or the high resolution interface capturing scheme by Muzaferija and Peric (21). Notably, there are also geometric VOF methods with support for complex geometries (22) with the potential of capturing the interface evolution at high accuracy. These are considered beyond the scope of the present study.

The coupling between volumetric phase fraction and linear momentum transport, Eqs. (2) and (3), is accomplished in a momentum conservative manner. The mass flux is reconstructed from the discretized transport equation for the advection of the volumetric phase fraction and consistently used after the solution of Eq. (2) with the update of mixture quantities in the convection term of the discretized linear momentum equation.

The time step is chosen such to fulfill the Courant-Friedrichs-Lewy condition based on the fluid, interface, and capillary velocity. The latter is employed to reduce spurious velocities, and is defined as (23)

$$Co_{cap} = \sqrt{\frac{2\pi\sigma}{\left(\rho_g + \rho_l\right)V}} \Delta t \tag{6}$$

with V denoting the mean cell volume and  $\Delta t$  the time step.

### Boundary and initial conditions

TABLE I. Geometry.

TABLE 1. Geometry.		
Dimension	Length (mm)	
$l_{ch}$	4.5	
$l_{ch,i}$	2.0	
$l_{ch,o}$	2.0	
$h_{ch}$	0.5	
b	0.5	
$l_{ptl}$	0.5	
$l_{pil} \ h_{ptl}$	0.1	

**TABLE II.** Fluid properties, from ref. (24)

Quantity	Symbol	Value
Liquid density	$\rho_l$	983 kg/m <sup>3</sup>
Liquid kinematic viscosity	$oldsymbol{ u}_l$	$0.475 \times 10^{-6} \text{ m}^2/\text{s}$
Gas density	$ ho_g$	$1.06 \text{ kg/m}^3$
Gas kinematic viscosity	$v_g$	$1.89 \times 10^{-5} \text{ m}^2/\text{s}$
Surface tension	σ	0.0644 N/m

At the inlet, pure gas is injected with U = 10 m/s and  $\alpha_l = 0$ . It is presumed that at the PTL/electrode boundary, liquid water is produced and oxygen is consumed. The effects of osmotic drag and membrane diffusion are not considered here, i.e., water is produced by the reaction only. Under the circumstances the net (mixture) mass flux is that due to hydrogen protons and electrons, namely;

$$\dot{m}_{\rm H_2} = 9\dot{m}_{\rm H_2O} - 8\dot{m}_{\rm O_2} \tag{7}$$

The choice of  $\alpha_l = 9$  and  $\alpha_g = 1$  -  $\alpha_l = -8$ , renders the correct value of U in Eq. (7) while satisfying the requirement  $\alpha_l + \alpha_g = 1$ . It is to be noted that this is a boundary value for  $\alpha_l$ , not an interior value, where  $0 \le \alpha_l \le 1$  and  $0 \le \alpha_g \le 1$  must strictly hold, at all times. The prescription is to be considered a purely numerical formulation for a counter-flow rather than a co-flow boundary condition, which would always result from  $0 \le \alpha_l \le 1$  values. This distinguishes the present work from the recent work of Niblett et al. (13) where only water drainage was considered in the PTL. The reader will note that Eq. (7) is consistentwith the so-called transferred-substance-state (T-state) formulation first formulated by Spalding (25) for both single-phase and multi-phase chemically-reacting mass transfer problems, as are found in catalytic converters, stirred tanks, and numerous other process engineering applications and equipment. The interested reader can find a discussion of the subject in Beale et al. (26). At the channel and PTL walls, as well as on the individual fibres, the static contact angle was fixed, as prescribed in Table III. For the initial fields, in the channel  $U = U_{in}\hat{i}$ ,  $\alpha_I = 0$  whereas in the PTL values of  $U = U_{el}\hat{j}$ ,  $\alpha_I = 0.5$  were selected ( $\hat{i}$  and  $\hat{j}$  are unit vectors in the x and y directions). The matter is discussed further, below.

TABLE III. Boundary conditions.

· · · · · · · · · · · · · · · · · · ·		
Description	Symbol	Value
Inlet mixture velocity	$U_{in}$	10 m/s
Electrode mixture velocity	$U_{ m el}$	0.1 m/s
Inlet liquid volume fraction	$\alpha_l$	0
Electrode liquid volume fraction	$lpha_{ m el}$	9
PTL fibre contact angle	$ heta_{ m f}$	150°
PTL box contact angle	$ heta_{ m w}$	150°
Gas channel base contact angle	$\Theta_{\mathrm{b}}$	150°
Gas channel top and sides contact angle	$ heta_{ ext{ts}}$	150°

# Code and implementation

The open source library OpenFOAM version 7 was employed to obtain solutions to the problem described above.

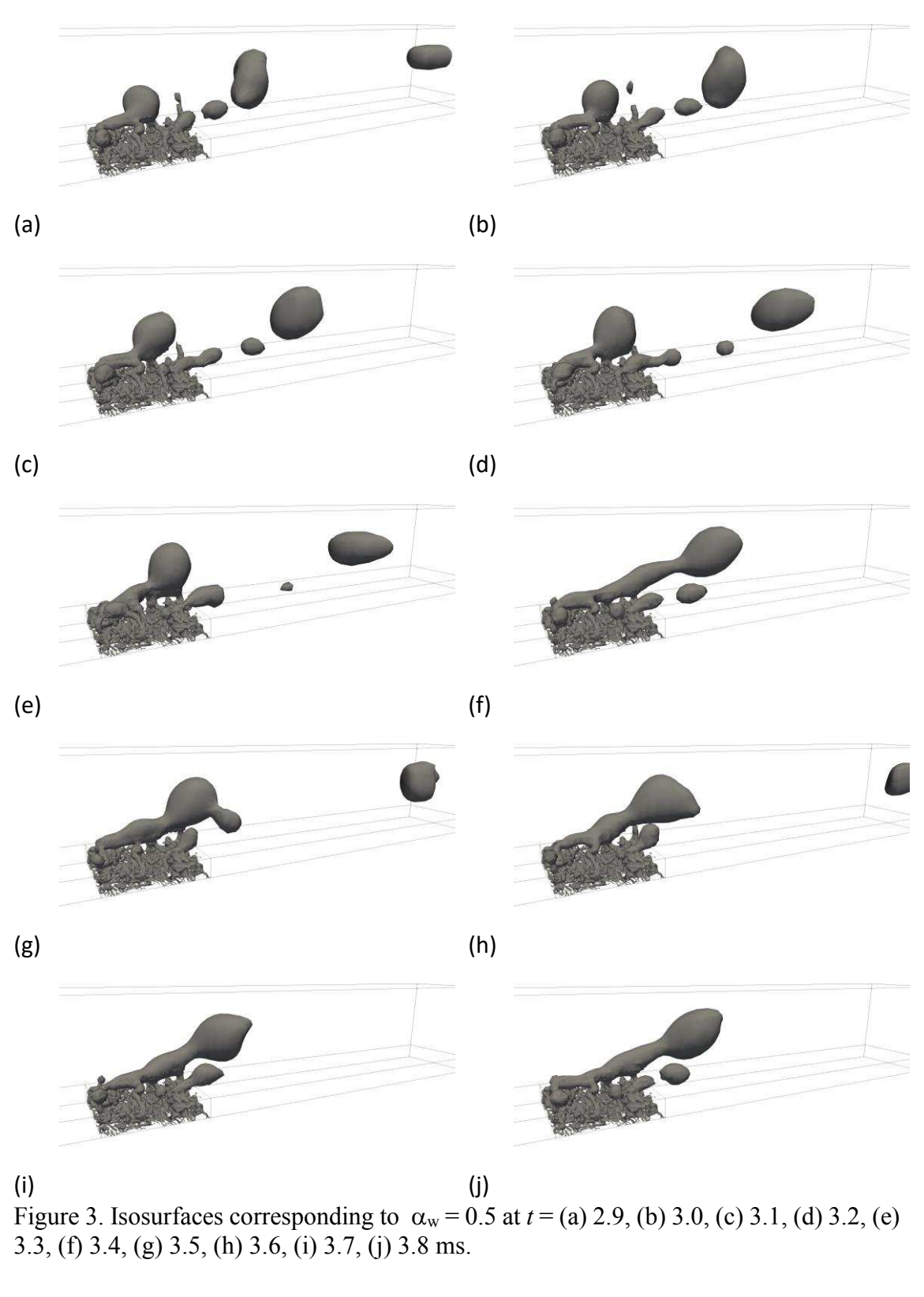
#### **Results**

The results, in terms of drop formation, are shown in Figure 3(a)-(j). It can be seen that following an initial transient, the drops are shed from the PTL into the channel, in a fairly regular manner, with a certain amount of spatial and temporal randomness. Fig. 4(a) shows spot values of water volume fraction,  $\alpha_w$ , at point P, Fig. 1, as a function of time. Figure 4(b) displays similar values of pressure, p (Pa). It can be seen that the pressure rises and falls as liquid drops pass through point P.

## **Discussion**

The numerical calculations indicate that though the creation, growth, and subsequent detachment of liquid drops at the PTL/gas channel interface is reasonably periodic: Yet there is also a certain element of randomness associated with the interactions between the different liquid streams at the PTL-channel interface. This leads to macro-scale fluctuations within the PTL near the channel as the drops are formed. However, within the bulk of the interior of the PTL, towards the electrode, the flow is relatively steady, as indeed would be expected for low Reynolds number flow exhibited in porous media.

The results show that the model is capable, not only of quantifying the two-phase flow of gas and liquid drops, as they are injected into, and convected downstream in the channel by the gas, but also importantly, of dispersing/separating the two-phases within the PTL. Even though the two phases at the electrode boundary are to be considered homogeneous, within the PTL they separate into two heterogeneous liquid and gas phases on a (continuum) micro-scale. This differentiation corresponds to physical reality in that the length scale of the electrochemical reaction at the oxygen electrode of a PEFC is one or two orders of magnitude smaller than the pore sizes in the PTL.



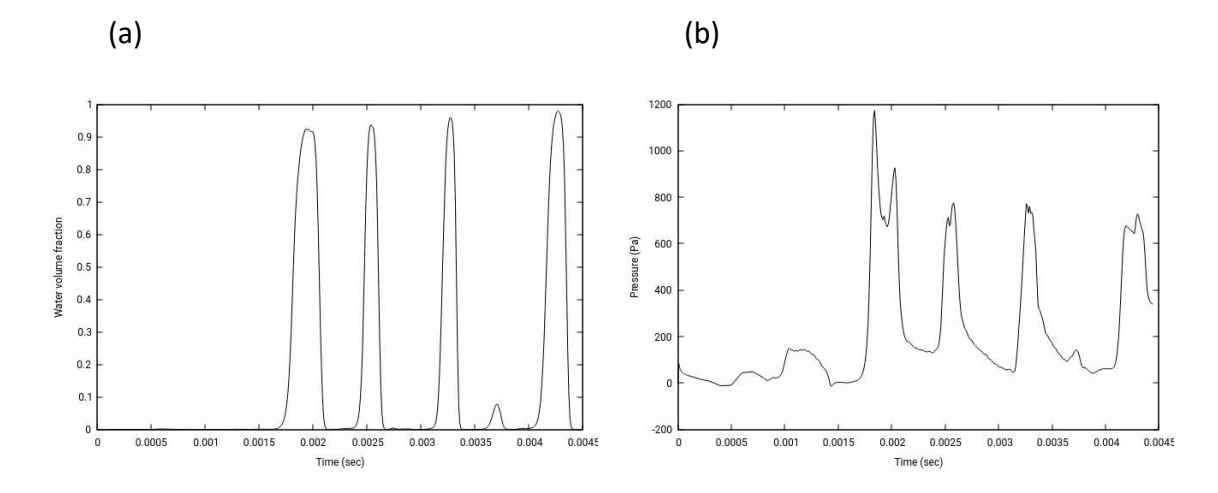


Figure 4. Spot values of (a) water volume fraction,  $\alpha_w$ , and (b) pressure, p (Pa), as a function of time, at point P, located in the centre of the gas channel midway between the porous transport layer specimen and the gas outlet.

This proof-of-concept is exciting as it can lead to series of parametric studies and eventual optimization of the PTL and related micro-porous structures. Some parameters that can be varied include channel-wall and PTL contact angles, and gas and mixture velocities. The reader will note that the T-state prescription for the gas/liquid, Eq. (7) at the electrode may be expressed in a more general form as  $\alpha_l = (9+18\beta)/(1+18\beta)$ ,  $\alpha_g = -8/(1+18\beta)$  where  $\beta$  is a net drag coefficient, that is the net number of water molecules dragged to/from the electrode because of protonic drag, back-diffusion, and convection/pressure gradient (27). Another family of problems amenable to the present analysis are water-electrolyzers which when operated with liquid water as feedstock, generate gas bubbles at the oxygen electrode. Such studies could be useful in identifying multi-phase flow regime changes as a function of gas flow velocity and current density.

### Numerical issues

The code consumed numerous weeks of time running in parallel (48 cores). This results from the requirement to keep the Courant number, Co < 1, and this is due to the fact that some pore sizes can be very small in the PTL. The choice of initial  $\alpha$ -fields is important from a convergence perspective: The heterogeneous reaction can only physically take place if both oxygen and water (and also protons) are simultaneously present at the electrode-PTL boundary. The prescriptions  $\alpha_l = 1$  (fully-wet) or  $\alpha_l = 0$  (empty-dry) at t = 0 within the PTL, may be problematic: Although the T-state  $\alpha$ -boundary condition will correctly drive interior  $\alpha$ -values to equilibrium values, in the range  $0 < \alpha < 1$ , there is no guarantee that during the initial transient, interior values outside these limits, could arise. If the solver then imposes the limits [0,1] on the  $\alpha$ -solution field, as is common, then divergence may arise. It is therefore recommended that these initial conditions be avoided for the problemat-hand.

#### **Conclusions**

The VOF method has successfully been applied to two-phase liquid-gas counter-flow in a PTL, with associated co-flow in the gas channel. The inlet/outlet boundary condition for the homogeneous gas/liquid production/destruction at the electrode led to a physically reasonable solution both in the PTL and the channel. The T-state concept was used to prescribe the counterflow mass fluxes of gas and liquid at the oxygen electrode. In the channel, where co-flow was observed, the continuous gaseous phase entrained the dispersed liquid phase in the form of drops which are subsequently advected to the outlet. The flow was periodic with some spatial and temporal randomness.

#### **Future work**

The properties of oxygen and water were selected for the two phases considered here, i.e., two-phases each composed of a single species. In fact, for a fuel cell, the composition of atmospheric air varies as oxygen is consumed,  $\rho_g = \rho_g \left( y_{O_2}, y_{N_2}, \ldots \right)$ . Therefore, conservation of species would add one or more additional scalar equations, for a multiphase, multi-species formulation. Moreover, as discussed by Gurau et al. (6), phase change issues, in the form of evaporation/condensation mass transfer are important and lead to water vapor being present in the gas phase. Calculation of inter-phase mass transfer requires the latent heat of evaporation/condensation based on the inter-phase temperature gradients to be prescribed. Hence, not only must the energy equation and individual species continuity equations also be solved, but also, some additional coding is required in the numerical scheme.

Experimental validation is a complex and important subject. The random nature of the PTL makes construction of repeatable experimental prototypes difficult or impossible, presently. Therefore, it is likely that any experimental research program would commence with samples of rectilinear matrices of circular cylinders for the PTL specimen. The diameter and pitch would be chosen so as to generate reasonable values of porosity and permeability. In addition to flow visualization studies, pressure measurements in the channel and elsewhere could be undertaken in conjunction with a power-spectral analysis of the drop-shedding frequency, as a function, say, of gas/liquid velocity, surface tension, and geometry.

The relatively coarse mesh generated, based on castellated octree refining, was deliberately employed to obtain solutions on a reasonably orthogonal framework. In the future, superior meshes employing surface snapping, and layer insertion will be constructed. These will rapidly increase the mesh size, with the potential for further reducing the Courant limit. A balance needs to be struck between mesh independence and available computational capabilities. This was always true, however, resources were scarcer in the past than today. Indeed, massively parallel computers should eventually allow for the PTL region to extend the entire length of the channel, at least for reasonably short channels. The development of a systematic methodology to optimize code parameters with an objective function of minimizing convergence time would be of great utility. This could be based on artificial intelligence/machine learning (28), possibly combined with mesh adaptation. The eventual goal would be to enable detailed simulations of real-size flow channels in single

cells. In this manner, water management, an extremely important issue in PEFC technology, can be improved by detailed mathematical modelling on a micro-scale.

### Acknowledgements

The authors wish to thank Mr. Eugen Hoppe for constructing a stereolithography file of the porous material used in this study. Discussions with Prof. Bedii Özdemir on the subject matter of the paper and on computational issues, were constructive. Calculations were performed on the high performance computing hardware of the Jülich Aachen Research Alliance (JARA), under grant number JARA0070.

### References

- 1. C. W. Hirt and B. D. Nichols, *J. Comput. Phys.*, **39**(1) 201-225 (1981).
- 2. F. H. Harlow and A. A. Amsden, *J. Comput. Phys.*, **8**(2) 197-213 (1971).
- 3. C. T. Crowe, M. P. Sharma, and D. E. Stock, *J. Fluids Eng.*, **99**(2) 325-332 (1977).
- 4. C. Wang and P. Cheng, *Int. J. Heat Mass Tran.*, **39**(17) 3607-3618 (1996).
- 5. C. Wang and P. Cheng, Advances in heat transfer, **30** 93-196 (1997).
- 6. V. Gurau, T. A. Zawodzinski, and J. A. Mann, J. Fuel Cell Sci. Technol., 5(2) 021009 (2008).
- 7. D. B. Spalding, Numerical Computation of Multi-phase Flow and Heat Transfer, in *Recent Advances in Numerical Methods in Fluids*, C. Taylor, Editor, pp. 139-167, Pineridge Press, Swansea (1980).
  - 8. A. D. Le and B. Zhou, *J. Power Sources*, **182**(1) 197-222 (2008).
- 9. M. Andersson, S. B. Beale, U. Reimer, W. Lehnert, and D. Stolten, *Int. J. Hydrogen Energy*, **43**(5) 2961-2976 (2018).
- 10. M. Andersson, A. Mularczyk, A. Lamibrac, S. B. Beale, J. Eller, W. Lehnert, and F. N. Büchi, *J. Power Sources*, **404** 159-171 (2018).
  - 11. M. Andersson, S. B. Beale, and W. Lehnert, eTransportation, 1 100003 (2019).
- 12. M. Andersson, V. Vukčević, S. Zhang, Y. Qi, H. Jasak, S. B. Beale, and W. Lehnert, *Int. J. Hydrogen Energy*, **44**(21) 11088-11096 (2019).
- 13. D. Niblett, A. Mularczyk, V. Niasar, J. Eller, and S. Holmes, *J. Power Sources*, **471** 228427 (2020).
  - 14. D. Deising, H. Marschall, and D. Bothe, *Chem. Eng. Sci.*, **139** 173-195 (2016).
  - 15. C. Dopazo, J. Fluid Mech., **81**(3) 433-438 (1977).
- 16. J. U. Brackbill, D. B. Kothe, and C. Zemach, *J. Comput. Phys.*, **100**(2) 335-354 (1992).
  - 17. J. P. Boris and D. L. Book, J. Comput. Phys., 11(1) 38-69 (1973).
  - 18. S. T. Zalesak, *J. Comput. Phys.*, **31**(3) 335-362 (1979).
  - 19. M. Rudman, Int. J. Numer. Methods Fluids, 24(7) 671-691 (1997).
  - 20. O. Ubbink and R. Issa, *J. Comput. Phys.*, **153**(1) 26-50 (1999).
- 21. M. Peric and S. Muzaferija, Computation of Free-Surface Flows using Interface-Tracking and Interface-Capturing Methods, in *Advances in Fluid Mechanics*, O. Mahrenholtz and M. Markiewicz, Editors, Computational Mechanics Publications, Southampton (1998).
  - 22. T. Marić, D. B. Kothe, and D. Bothe, J. Comput. Phys., **420** 109695 (2020).
- 23. P. Personnettaz, P. Beckstein, S. Landgraf, T. Köllner, M. Nimtz, N. Weber, and T. Weier, *J. Power Sources*, **401** 362-374 (2018).
  - 24. D. R. Lide, CRC Handbook of Chemistry and Physics. Vol. 85. CRC press (2004).

- 25. D. B. Spalding, Int. J. Heat Mass Tran., 1 192-207 (1960).
- 26. S. B. Beale, S. Zhang, M. Andersson, R. T. Nishida, J. G. Pharoah, and W. Lehnert, Heat and Mass Transfer in Fuel Cells and Stacks, in *50 Years of CFD in Engineering Sciences: A Commemorative Volume in Memory of D. Brian Spalding*, A.K. Runchal, Editor, pp. 485-511, Springer, Singapore (2020).
  - 27. S. B. Beale, Int. J. Hydrogen Energy, 40(35) 11641-11650 (2015).
- 28. A. K. Runchal and M. M. Rao, CFD of the Future: Year 2025 and Beyond, in 50 Years of CFD in Engineering Sciences: A Commemorative Volume in Memory of D. Brian Spalding, A.K. Runchal, Editor, pp. 779-795, Springer, Singapore (2020).